



ELSEVIER

Available online at www.sciencedirect.com

ScienceDirect

<http://www.elsevier.com/locate/biombioe>

Application of an empirical model in CFD simulations to predict the local high temperature corrosion potential in biomass fired boilers

Thomas Gruber ^{a,*}, Robert Scharler ^{a,b,c}, Ingwald Obernberger ^{b,c}

^a BIOENERGY 2020+ GmbH, Inffeldgasse 21b, 8010 Graz, Austria

^b Institute for Process and Particle Engineering, Graz University of Technology, Inffeldgasse 13, 8010 Graz, Austria

^c Bios Bioenergiesysteme GmbH, Inffeldgasse 21b, 8010 Graz, Austria

ARTICLE INFO

Article history:

Received 17 July 2014

Received in revised form

19 February 2015

Accepted 20 February 2015

Available online xxx

Keywords:

Biomass combustion

Combined heat and power generation (CHP)

Corrosion

Model

Wood chips

ABSTRACT

To gain reliable data for the development of an empirical model for the prediction of the local high temperature corrosion potential in biomass fired boilers, online corrosion probe measurements have been carried out. The measurements have been performed in a specially designed fixed bed/drop tube reactor in order to simulate a superheater boiler tube under well-controlled conditions. The investigated boiler steel 13CrMo4-5 is commonly used as steel for superheater tube bundles in biomass fired boilers. Within the test runs the flue gas temperature at the corrosion probe has been varied between 625 °C and 880 °C, while the steel temperature has been varied between 450 °C and 550 °C to simulate typical current and future live steam temperatures of biomass fired steam boilers. To investigate the dependence on the flue gas velocity, variations from $2 \text{ m} \cdot \text{s}^{-1}$ to $8 \text{ m} \cdot \text{s}^{-1}$ have been considered. The empirical model developed fits the measured data sufficiently well. Therefore, the model has been applied within a Computational Fluid Dynamics (CFD) simulation of flue gas flow and heat transfer to estimate the local corrosion potential of a wood chips fired 38 MW steam boiler. Additionally to the actual state analysis two further simulations have been carried out to investigate the influence of enhanced steam temperatures and a change of the flow direction of the final superheater tube bundle from parallel to counter-flow on the local corrosion potential.

© 2015 Elsevier Ltd. All rights reserved.

1. Introduction

High temperature corrosion processes have a strong influence on the operation of biomass fired boilers and result in unscheduled outages and reduced economic efficiencies. Still, the high temperature corrosion of superheaters in biomass combustion plants is insufficiently explored so far. A wide

range of experimental data exists, where the effect of deposits of certain species, such as NaCl or KCl or the influence of single parameters such as flue gas temperature or steel temperature has been investigated (e.g. Refs. [1–5]). These experiments are not sufficient to describe the high temperature corrosion processes in real-scale plants accurately, due to the interaction and the high complexity of the processes involved. High temperature corrosion in real scale biomass fired plants

* Corresponding author. Tel.: +43 0 316 873 9228; fax: +43 0 316 873 9202.

E-mail address: thomas.gruber@bioenergy2020.eu (T. Gruber).

<http://dx.doi.org/10.1016/j.biombioe.2015.02.024>

0961-9534/© 2015 Elsevier Ltd. All rights reserved.

has been investigated by several authors (e.g. Refs. [6–9]). Measurements in real scale plants generally have the drawback that it is not possible to vary parameters of interest arbitrarily. For these reasons no experimental data are available so far which are sufficient to develop a reliable simulation tool to calculate the local corrosion potential in biomass fired plants.

2. Objectives

The aim of the work presented is the application of a newly developed empirical model [10] together with a CFD simulation of flow and heat transfer to calculate the local high temperature corrosion potential in a biomass fired steam boiler. In addition to the actual state analysis the influences of enhanced steam temperatures as well as a change of the flow direction of the final superheater tube bundle from parallel to counter-flow on the local corrosion potential is investigated within this work.

3. Methodology

To enhance the readability of the work the basic principles of the experimental approach as well as the model development already presented in Ref. [10] are summarized in the sections 3.1–3.4 as detailed as necessary.

3.1. Combined biomass fired packed bed/electrically heated drop tube reactor

The experiments have been carried out using a combined packed bed/drop tube reactor, with which well-defined conditions regarding flue gas temperature and composition, typically prevailing in biomass fired boilers, can be achieved. A schematic view of the reactor can be found in Fig. 1. The setup applied consists of a packed bed reactor (biomass grate furnace with air staging and flue gas recirculation), an upper transition part to a successively heated vertical tube with isothermal conditions (the so-called drop tube). The drop tube has an electrical input power of 60 kW and allows the control of the flue gas temperature between 625 °C and 900 °C. The power input of the drop tube allows a compensation of the fluctuation of the grate furnace operation and, therefore, to achieve constant and adjustable flue gas temperatures in front of the corrosion probe. The drop tube has a length, which is sufficient to get a fully developed flow at the entrance to the measurement port, which is equipped with the corrosion probe. Therefore, the reactor enables corrosion measurements under defined flow and temperature conditions with a flue gas composition typical for fixed bed combustion systems. Finally, the flue gas is transferred via a lower transitional part to a water cooled heat exchanger before it enters the chimney. A detailed description of the setup used can be found in Ref. [10].

The experimental setup allows variations of the parameters of interest independently from each other. The flue gas temperature is varied by the electrical heating of the drop tube, the flue gas velocity is varied by the furnace load

conditions, whereas the steel temperature is varied by the air cooling of the probe.

3.2. Online corrosion probe measurement

The online corrosion probe measurement technique applied within the test runs was developed and provided by Corromoran GmbH, Augsburg, Germany. It is especially designed to simulate the high temperature corrosion occurring on superheater tubes. The corrosion probe is inserted into the flue gas at the measuring port below the electrically heated drop tube. It consists of a temperature controlled sensor placed on the top of an air cooled carrier lance. When exposed to the flue gas, a layer consisting of deposits and corrosion products is formed on the sensor surface. This layer represents an electrolyte and allows the measurement of a linear polarization resistance, which is proportional to the instantaneous corrosion rate. The factor describing the relation between the linear polarization resistance and the corrosion rate is determined subsequently to the test run by a gravimetric measurement of a mass loss ring. A detailed description of the probe can be found in Refs. [11] and [12].

The corrosion probe used has already been successfully applied in waste incinerators [11,13] as well as biomass fired boilers [12].

It should be mentioned that the corrosion rates measured within this work give only qualitative information about the corrosion potential in dependence of relevant operating parameters. High temperature corrosion is a strongly time-dependent process which often follows a parabolic or parabolic trend [14]. Therefore, the corrosion rates gained within short-term measurements generally differ from those found within long-term measurements. Nevertheless, short-term online corrosion measurements still allow the investigation of the dependence on a certain parameter.

3.3. Corrosion probe test campaign

The fuel used in the test campaign was chemically untreated forest wood chips mainly consisting of spruce (lat. *picea abies*). The biomass mostly consists of logging residues, but also contains stem wood and bark as well as a low fraction of needles and fine particles. A photo of the fuel is given in Fig. 2. The fuel was taken from the storage of the biomass combined heat and power plant Baden (Lower Austria, Austria), which uses biomass harvested in the forests in a radius of approximately 50 km around Baden. Before the wood chips could be used in the coupled fixed bed/drop tube reactor, described in Section 3.1, the particle size had to be reduced by chopping from P63^c to P45A^c according to EN 14961-1:2010. The resized wood chips were stored for 1–7 weeks, depending on their time of usage, in several 1 m³ plastic big bags before they were fired in the biomass reactor. The wood chips used within the test campaign had following specifications according to EN 14961-1:2010: origin ... 1.1.4.4 and 1.1.4.5 (logging residues), particle ... P45A^C, moisture ... M25, ash ... A3.0, bulk density ... BD200. The chemical composition of the wood chips can be found in Table 1. The three samples for the fuel analyses have been taken at different times over the whole test campaign from the fuel storage of the biomass reactor.

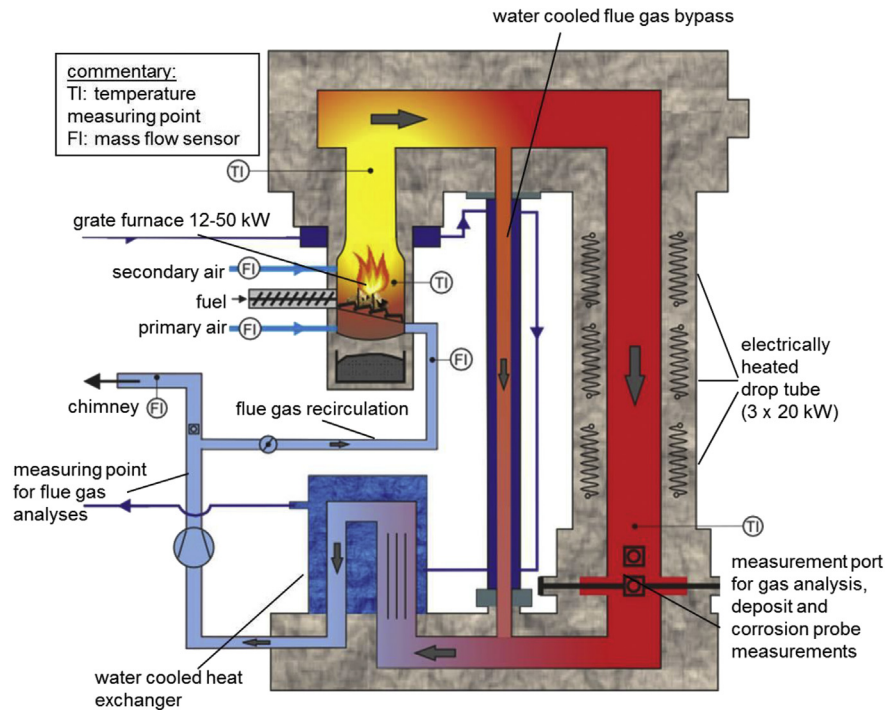


Fig. 1 – Schematic view of the combined packed bed/drop tube reactor with relevant units and measurement ports [10].

A detailed description of the test campaign methodology and boundary conditions can be found in Ref. [10]. Nevertheless, the most important parameters are listed in Tables 2 and 3.

The investigated boiler steel 13CrMo4-5 is commonly used as steel for superheater tubes in biomass fired heat and power plants. The operating duration of the biomass reactor was 325 h. After a startup time which was used to achieve a reproducible signal, the parameter variations listed in Table 2 have been performed.



Fig. 2 – Picture of the biomass fuel used for the test runs.

3.4. Model development

Origin of the model development was a sensitivity analysis of relevant influencing parameters. Based on this analysis, the parameters of the model function (see section 4.2) were

Table 1 – Chemical composition of the fuel investigated.
 Explanation: mean ... mean value, std-dev ... standard deviation, w.b. ... wet basis, d.b. ... dry basis; number of samples = 3; the concentrations of the elements C, H and N have only been determined from one representative sample.

	Mean	Std-dev	Unit
Moisture content	0.241	0.036	Mass fraction w.b.
Ash content	0.024	0.007	Mass fraction d.b.
C	0.481	–	Mass fraction d.b.
H	0.059	–	Mass fraction d.b.
N	0.003	–	Mass fraction d.b.
S	280	8	mg·kg ⁻¹ d.b.
Cl	90	18	mg·kg ⁻¹ d.b.
Si	2122	1382	mg·kg ⁻¹ d.b.
Ca	6045	998	mg·kg ⁻¹ d.b.
Mg	739	369	mg·kg ⁻¹ d.b.
K	1660	147	mg·kg ⁻¹ d.b.
Na	63	15	mg·kg ⁻¹ d.b.
P	204	18	mg·kg ⁻¹ d.b.
Al	446	171	mg·kg ⁻¹ d.b.
Fe	265	77	mg·kg ⁻¹ d.b.
Mn	108	54	mg·kg ⁻¹ d.b.
Zn	19	1	mg·kg ⁻¹ d.b.
Pb	1	0	mg·kg ⁻¹ d.b.
Molar 2S/Cl ratio	6.9	0.6	mol·mol ⁻¹

Table 2 – Range of parameter variations performed.

	Unit	Min	Max
Steel temperature	°C	450	550
Flue gas temperature	°C	625	880
Flue gas velocity	m·s ⁻¹	2	8

determined by a stepwise minimization of the quadratic errors for all influencing parameters.

3.5. CFD models used and heat exchanger model

Following models have been used in the CFD simulation: Realizable k- ϵ model with enhanced wall functions (turbulence) and the Discrete Ordinates model (radiation).

In the last decade the computational performance strongly increased. A detailed CFD simulation of the convective boiler section with a resolution of the heat exchanger tubes is still impossible within a reasonable time due to the large variations of geometric length scales and transient flow phenomena like vortex shedding behind tubes. Therefore, a finite cell based convective heat exchanger model has been developed by BIOS BIOENERGIESYSTEME GmbH, Graz, Austria in order to investigate the whole boiler by means of CFD simulations. A detailed description of the model can be found in Ref. [15].

The heat exchanger model was applied in order to calculate the flow as well as the convective and radiant heat transfer in the superheater tube banks. The calculation of the source terms for momentum and energy transport equations is based on literature data [16–18]. These data are available for tube banks of staggered and in-line arrangement and flow perpendicular to the individual tube rows. Transient 2D simulations were performed to calculate the flow resistance for flow directions other than the literature values. Thus, the dependence of flow resistance on the flow angle within a tube bank can correctly be accounted for [15].

For these reasons the heat exchanger model is well suited to calculate the heat transfer in heat exchangers passed through by flue gas with an inhomogeneous flow field.

3.6. Case study description

To test and verify the model developed, it has been applied for a CFD simulation of flow and heat transfer in a 42 MW_{th} wood chips fired CHP plant. The high temperature corrosion potential on the superheater bundles has been calculated for three different cases:

- **CS1:** Actual state analysis under full load conditions (live steam temperature of 453 °C)

Table 4 – Relevant boiler information.

Fuel power input related to NCV	41.9	MW
Boiler output	37.8	MW
Flue gas mass flow	35.6	kg·s ⁻¹
Saturated steam temperature	279	°C
Saturated steam pressure	6300	kPa
Live steam temperature	453	°C
Live steam pressure	6100	kPa

- **CS2:** A switch of the flow direction of the final superheater bundle from parallel to counter-flow (live steam temperature of 453 °C)
- **CS3:** Enhanced live steam temperature of 480 °C

Table 4 provides the most relevant operating conditions of the boiler; whereas Table 5 provides relevant information regarding the superheater tube bundles.

The steel 16Mo3 used for the superheaters of the plant is a low alloy heat resisting steel like 13CrMo4-5 with a low Cr and Ni content and, therefore, should show a comparable corrosion behavior.

The simulation has been performed within a two-step approach. First, the flue gas flow and heat transfer of the boiler was simulated. Afterwards, the local corrosion behavior was evaluated in a post-processing step.

The boundary conditions (e.g. flue gas temperature and composition) at the entrance of the simulation domain were taken from mass and energy balances under the assumption of complete combustion provided by the plant manufacturer.

To achieve a fully developed flow-field at the entrance to the convective boiler section, the upper part of the furnace was included in the simulation. Hence, the simulation considers the composition of a chemically not reacting flue gas typical for biomass furnaces firing wood chips.

Furthermore, a linear increase of the steam temperature within the superheater tube bundles was assumed.

The heat loss over the finned tube walls is calculated by the saturated steam temperature and the mean heat transfer coefficient on the water side as boundary conditions.

To consider the reduced heat transfer due to ash deposits on the tubes a thermal resistance of 2 m² K·kW⁻¹ is assumed (low fouling rate) on the finned tube walls and the superheater tube walls.

Fig. 3 illustrates the different sections of the biomass CHP plant considered in the CFD case study. The simulation domain comprises the upper part of the furnace section, the radiative boiler section (including the two evaporator tube grids ET1 and ET2), the transition to the convective section,

Table 3 – Flue gas composition during the online corrosion probe measurements. Explanation: mean ... mean value over the balancing time, std-dev ... standard deviation over the balancing time.

	Mean	Std-dev	Unit
CO ₂	11.1	0.9	Vol.-% dry flue gas
O ₂	9.5	0.9	Vol.-% dry flue gas
CO	13.8	0.7	mg·m ⁻³ (at 0 °C and 101 325 Pa, dry flue gas, 13 Vol.-% O ₂)
SO ₂	8.6	2.8	mg·m ⁻³ (at 0 °C and 101 325 Pa, dry flue gas, 13 Vol.-% O ₂)
HCl	6.6	3.8	mg·m ⁻³ (at 0 °C and 101,325 Pa, dry flue gas, 13 Vol.-% O ₂)

Table 5 – Relevant boundary conditions for the superheater tubes. Explanation: SH1–SH3 ... superheater tube bundle 1–3, ccf ... cross counter flow, cpf ... cross parallel flow.

		SH1	SH2	SH3
Type	–	Bank of in-line tubes		
Operating mode	–	ccf	ccf	cpf
Outer tube diameter	mm	38	38	38
Tube wall thickness	mm	4	4	4
Tube wall material	–	16Mo3	16Mo3	16Mo3
Heating surface	m ²	396	396	198

the ash hopper as well as the convective section with the three superheaters SH1 to SH3.

4. Result and discussion

4.1. Selected results of corrosion probe measurements

The online corrosion measurements for the fuel forest wood chips showed an exponential dependence on the flue gas temperature as well as on the steel temperature (see Figs. 4 and 5). This result is in good agreement with long-term corrosion probe measurements performed at a CHP plant fired with forest wood chips [12]. Furthermore, a weaker, linear dependence could be found on the flue gas velocity (see Fig. 6). The experimental data were recorded over a period of several days and were well reproducible. Due to these facts, these short-term corrosion measurements at the test rig seem well applicable to develop an empirical

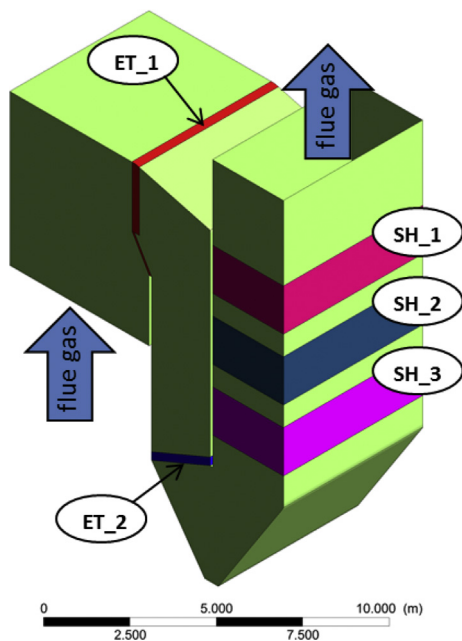


Fig. 3 – Schematic view of the simulated CHP plant. Explanation: ET_1 ... upper evaporator tube grid, ET_2 ... lower evaporator tube grid, SH_1 to SH_3 ... superheater tube bundles 1 to 3.

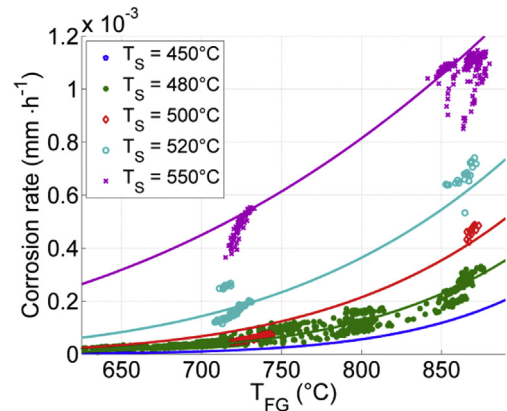


Fig. 4 – Plot of the measured corrosion rates (markers) and the empirical function developed (lines) as a function of the flue gas temperature for several steel temperatures [10]. Explanation: T_S ... steel temperature; T_{FG} ... flue gas temperature; the flue gas velocity has been kept constant to $2.8 \pm 0.5 \text{ m}\cdot\text{s}^{-1}$.

function, which can be used to calculate the local high temperature corrosion potential of real-scale biomass firing plants. A more detailed description of these results can be found in Ref. [10].

4.2. Empirical corrosion model

The model developed consists of an Arrhenius function, which describes the dependence on the flue gas and steel temperature, the influence of the flue gas velocity is taken into account by a linear function. The quality of the empirical model is shown in Figs. 4–6, where the measured data are compared with the function developed. The optimized coefficients of the empirical function are listed in Table 6.

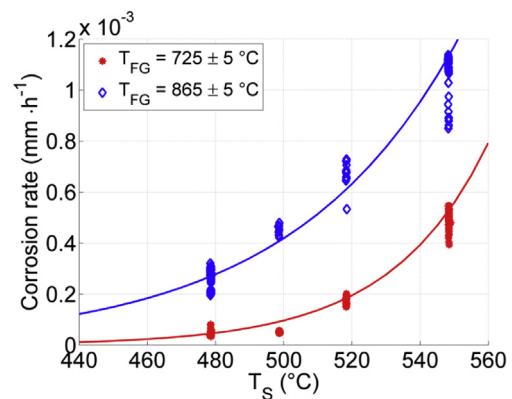


Fig. 5 – Plot of the measured corrosion rates (markers) and the empirical function developed (lines) as a function of the steel temperatures for several flue gas temperatures [10]. Explanation: T_{FG} ... flue gas temperature; T_S ... steel temperature; the flue gas velocity has been kept constant to $2.8 \pm 0.5 \text{ m}\cdot\text{s}^{-1}$.

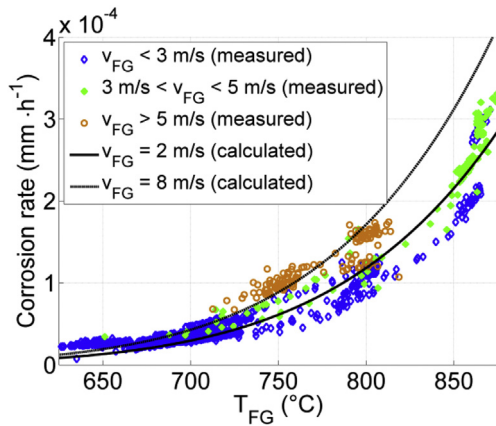


Fig. 6 – Trend of measured corrosion rates as a function of flue gas velocity and temperature (markers) in comparison to the values of the empirical function (lines) developed [10]. Explanation: v_{FG} ... flue gas velocity; T_{FG} ... flue gas temperature; the steel temperature has been kept constant at 480 ± 0.5 °C.

$$\text{CorrRate} = A(T_s) \cdot \exp\left(\frac{B(T_s)}{R \cdot T_{FG}}\right) \cdot \frac{C(v_{FG})}{1000} \quad (1)$$

$$A(T_s) = \exp(a_1 \cdot T_s + a_2) \quad (2)$$

$$B(T_s) = b_1 \cdot T_s + b_2 \quad (3)$$

$$C(v_{FG}) = c_1 \cdot v_{FG} + c_2 \quad (4)$$

with: CorrRate ... corrosion rate ($\text{mm} \cdot \text{h}^{-1}$), $A(T_s)$... max. corrosion rate ($\text{mm} \cdot \text{h}^{-1}$), $B(T_s)$... activation energy ($\text{J} \cdot \text{mol}^{-1}$), T_{FG} ... flue gas temperature (K), T_s ... steel temperature (K), v_{FG} ... flue gas velocity ($\text{m} \cdot \text{s}^{-1}$), R ... gas constant ($\text{J} \cdot \text{mol}^{-1} \cdot \text{K}^{-1}$), $a_{1-2}, b_{1-2}, c_{1-2}$... coefficients.

4.3. Application range of the empirical model

Generally, the empirical function developed is valid within the parameter range of the corrosion probe measurements (see Table 2) and can be applied for comparable corrosion mechanisms.

As discussed in detail in Ref. [10] no chlorine or traces of a molten layer could be found neither in the deposit nor the corrosion layer of the corrosion probe by means of SEM/EDX analyses. Therefore, it is suggested that the main corrosion mechanism prevailing is the oxidation of the low alloy steel by molecular oxygen.

Hence, for other corrosion mechanisms such as active Cl induced oxidation or corrosion by molten sulfates, the model is not validated.

Table 6 – Optimized coefficients of the empirical model [10].

a_1	a_2	b_1	b_2	c_1	c_2
-0.083	73.9	982	-858,364	0.07	0.81

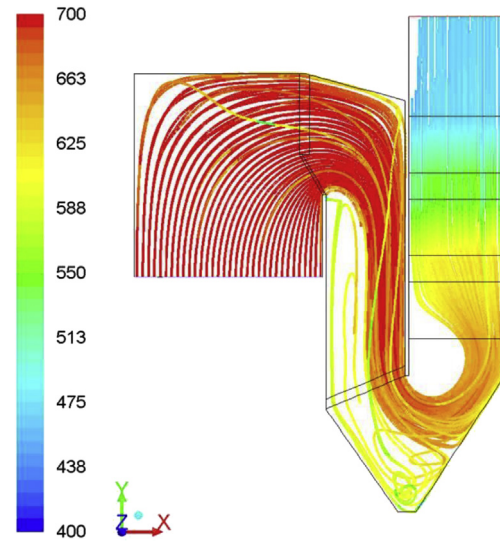


Fig. 7 – Streamlines of the flue gas colored by the temperature (°C) in the symmetry plan of the simulated plant (case CS1).

4.4. Results of the CFD simulations of flow and heat transfer

Since the calculated flow fields of CS2 and CS3 are qualitatively similar to the one of CS1 only results of CS1 are presented within this work.

The calculated flue gas path lines colored by the flue gas temperature for full load conditions are shown in Fig. 7, whereas the calculated flue gas velocities are presented in Fig. 8. The linearly increasing steam temperatures in the superheater bundles (boundary conditions) are presented in Fig. 9.

One can see that the flue gas passes along the right boiler wall of the superheater duct. Therefore, superheater 3 is not

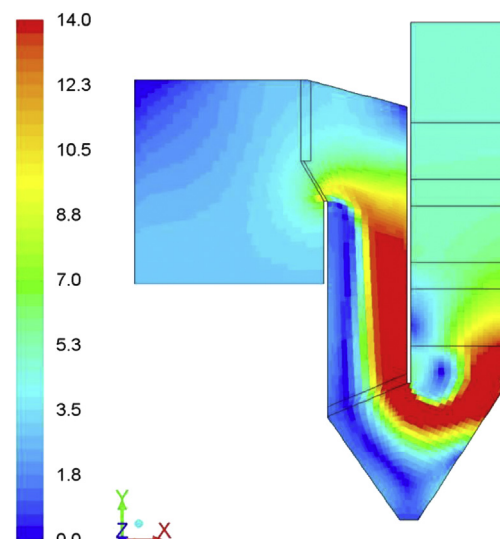


Fig. 8 – Flue gas velocity ($\text{m} \cdot \text{s}^{-1}$) in the symmetry plan of the simulated plant (case CS1).

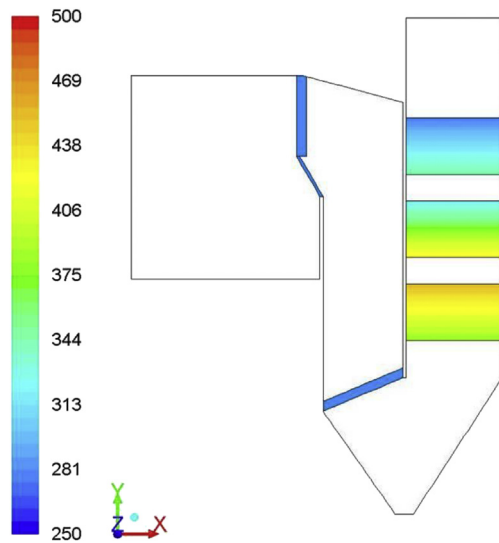


Fig. 9 – Plot of the linearly increasing steam temperatures (°C) in the symmetry plan of the simulated plant (case CS1).

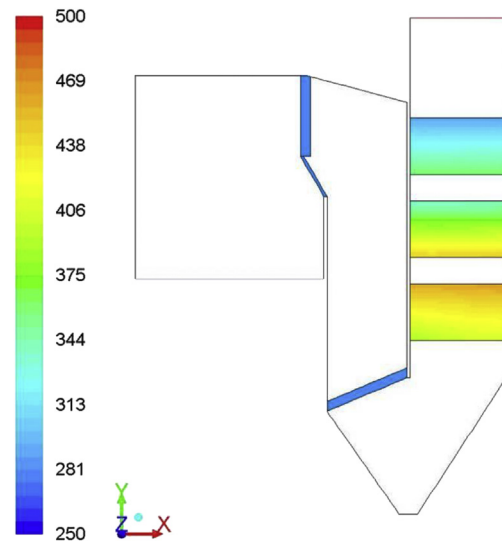


Fig. 11 – Steel temperature (°C) of the heat exchangers in the symmetry plan of the simulated plant (case CS1).

equally passed through by the flue gas. This leads to enhanced flue gas velocities and flue gas temperatures on the right side of the tube bundle and therefore, locally enhanced heat transfer coefficients on the flue gas side (see Fig. 10). Furthermore, it can be seen that superheater 3 homogenizes the flow distribution over the cross-section before the flue gas enters the superheater bundle 2.

The empirical model developed strongly depends on the local steel temperature. To calculate the local steel temperatures, the heat exchanger model uses the local values of steam temperature, local heat flux and the heat transfer coefficient on the flue gas side. Therefore, the calculated steel temperatures in this work take the effects of an inhomogeneous flow field into account. The calculated steel temperatures of the heat exchangers are shown in Fig. 11.

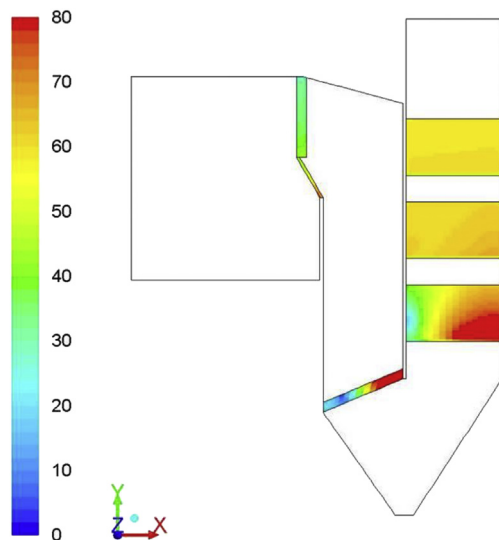


Fig. 10 – Heat transfer coefficient ($\text{W}\cdot\text{m}^{-2}\cdot\text{K}^{-1}$) on the flue gas side in the symmetry plan of the simulated plant (case CS1).

To investigate the influence of an inhomogeneous flow field on the convective heat transfer and the pressure loss over the superheater tube bundles the results of the CFD simulation for CS1 have been compared with calculations according to the VDI heat atlas [17] Gg1 (heat transfer) and IDELCHIK - Handbook of hydraulic resistance [16] p.752 (pressure loss). The results of this comparison are shown in Tables 7–9.

Due to the homogenous flow field in the superheater tube bundles 1 and 2 the calculated pressure losses according to the CFD simulation and the empirical calculation are in good agreement. For the bundles 1 and 2 there are deviations regarding the amount of transferred heat by convection, due to effects of the radiation, which is not considered in the empirical correlation. In case of the final superheater (SH3), the results concerning pressure loss and heat transfer differ considerably, since the velocity and temperature gradient predicted with the CFD simulation cannot be considered by the empirical correlations, which assume a homogenous flow through the bundle.

4.5. Application of the empirical high temperature corrosion model

The model has been applied in a post-processing step based on the already calculated temperature and flow profile of the CFD simulation.

Table 7 – Comparison of the transferred heat by convection and the pressure loss according to the CFD simulation and the calculations based on [16] and [17] for SH1.

	Unit	CFD	Calculations
Flue gas temperature SH entry	°C	536	536
Flue gas temperature SH exit	°C	469	463
Mean surface temperature	°C	366	366
Transferred heat by convection	kW	3035	3205
Pressure loss	Pa	44	46

Table 8 – Comparison of the transferred heat by convection and the pressure loss according to the CFD simulation and the calculations based on [16] and [17] for SH2.

	Unit	CFD	Calculations
Flue gas temperature SH entry	°C	610	610
Flue gas temperature SH exit	°C	541	536
Mean surface temperature	°C	442	442
Transferred heat by convection	kW	3087	3296
Pressure loss	Pa	50	51

The CFD simulations of flow and heat transfer show that flue gas temperatures as well as the steel temperatures in the superheater tube bundles 1 and 2 are below the application range of the empirical model. Therefore, the empirical model is only applied to calculate the local corrosion potential for the final superheater.

The calculated local corrosion potentials for the three different cases can be found in Figs. 12–14. Since already very small leaks of the superheater tubes lead to a shut-down of the boiler, the maximum values of the calculated corrosion potentials of the final superheater are compared in Table 10.

The sensitivity study shows that a switch of the flow direction of the final superheater from parallel to counter-flow increases the maximum of the corrosion potential by a factor of 3.4. This result can be explained by the combination of the highest surface temperature with an increased flue gas temperature in the first part of the superheater tube bundle. An increase of the live steam temperature by ~30 °C, from 453 °C to 480 °C, leads to a maximum corrosion potential which is 7.4 times higher than that found within the actual state analysis of the plant.

It is proposed that the main corrosion mechanism prevailing is the oxidation by molecular oxygen and hence, time dependent. Therefore, the corrosion rates shown in Table 10 and Figs. 6 to 8 should only be interpreted qualitatively. There might be deviations between the predicted rates according to the empirical model and the corrosion rates found in real CHP plants. Nevertheless, the data gained under well-defined conditions from short-term measurements can be used to determine trends and allow a comparison of different cases.

In general, the danger of a material failure of the superheater tubes under full load conditions can be considered as low. This is in good agreement with long-term observations of the plant operator. Also one can see that corrosion becomes considerably higher when the steam temperatures are increased.

Table 9 – Comparison of the transferred heat by convection and the pressure loss according to the CFD simulation and the calculations based on [16] and [17] for SH3.

	Unit	CFD	Calculations
Flue gas temperature SH entry	°C	646	646
Flue gas temperature SH exit	°C	616	612
Mean surface temperature	°C	480	480
Transferred heat by convection	kW	1678	1528
Pressure loss	Pa	20	40

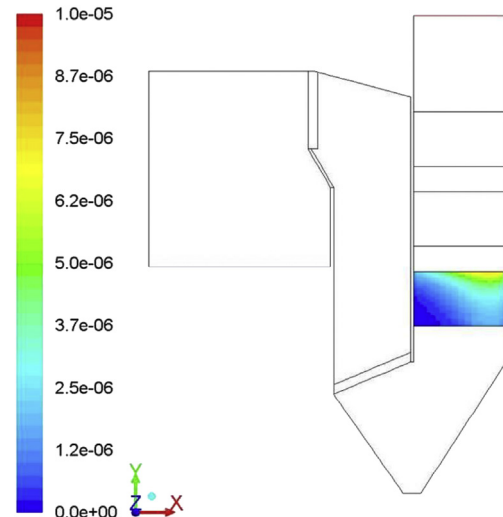


Fig. 12 – Calculated local corrosion potential ($\text{mm}\cdot\text{h}^{-1}$) of the superheaters in the symmetry plan of the simulated plant under full load conditions (CS1).

5. Summary and conclusion

To investigate the high-temperature corrosion behavior of superheater tube bundles, online corrosion probe measurements have been carried out in a specially designed fixed bed/drop tube reactor. The investigated boiler steel 13CrMo4-5 is commonly used as steel for superheater tubes in biomass fired heat and power plants. The reactor used allows an independent variation of a single parameter of interest. Therefore, the quality of the measured correlations between the corrosion probe signal and the influencing parameters exceeds those already published. The corrosion probe measurements show a clear dependence on the parameters flue gas temperature and

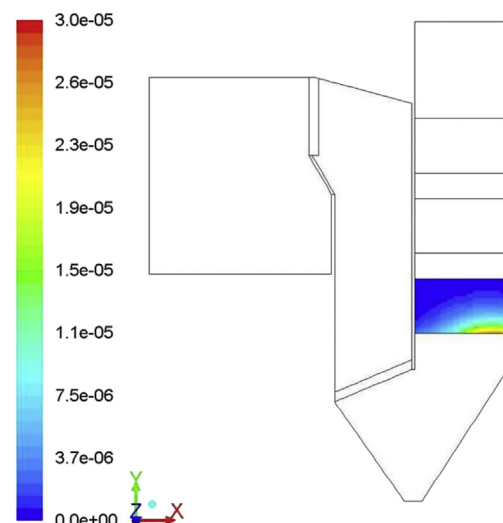


Fig. 13 – Calculated local corrosion potential ($\text{mm}\cdot\text{h}^{-1}$) of the superheaters in the symmetry plan of the simulated plant for a changed flow in the final superheater (CS2).

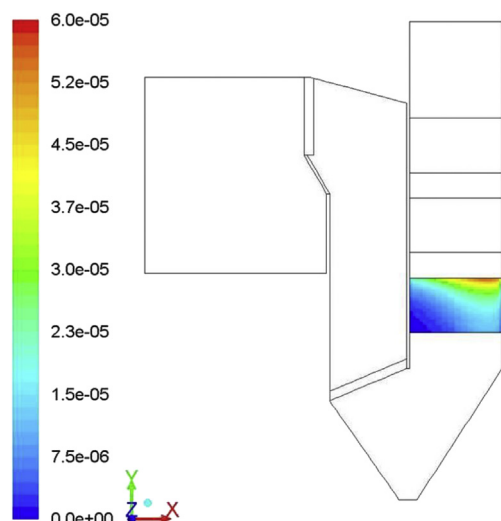


Fig. 14 – Calculated local corrosion potential ($\text{mm}\cdot\text{h}^{-1}$) of the superheaters in the symmetry plan of the simulated plant for enhanced steam temperatures (from $453\text{ }^{\circ}\text{C}$ to $480\text{ }^{\circ}\text{C}$) (CS3).

velocity as well as the steel temperature. The following variations have been carried out to investigate the influence on the corrosion behavior: flue gas temperature between $625\text{ }^{\circ}\text{C}$ and $880\text{ }^{\circ}\text{C}$, steel temperature from $450\text{ }^{\circ}\text{C}$ to $550\text{ }^{\circ}\text{C}$ and flue gas velocity from $2\text{ m}\cdot\text{s}^{-1}$ to $8\text{ m}\cdot\text{s}^{-1}$. Based on the experimental data gained, an empirical function has been developed which is a combination of an Arrhenius function describing the dependence on the flue gas and the steel temperature and a linear dependence on the flue gas velocity. This empirical function is able to reproduce the corrosion potential measured sufficiently accurate. The model is validated for the parameter range investigated within the test runs.

Although the model developed is not able to predict actual corrosion rates due to the fact that the measurement time of the test run has been kept rather short ($\sim 300\text{ h}$), the general dependence on the parameters is comparable to those found during long-term measurements in a real-scale, forest wood chips fired biomass steam boiler [12].

Some restrictions have to be made regarding the applicability of the model. The use of a Cr or Ni rich superheater material can affect the corrosion behavior considerably. The empirical model developed is only validated for low alloy superheater materials such as 13CrMo4-5 or 16Mo3. Furthermore, the corrosion behavior strongly depends on the corrosion mechanism. It is suggested that the main corrosion mechanism prevailing within this work is the oxidation of the steel by molecular oxygen. Deviations in the fuel composition can lead to different corrosion mechanisms such as active Cl-induced corrosion or corrosion by molten salts. Therefore, the application of the model is restricted to chemically untreated

wood chips as fuel. To increase the validity range of the model additional measurements with different superheater materials and different types of herbaceous fuels or agricultural residues should be performed.

The newly developed model has been applied within a CFD simulation of flow and heat transfer to calculate the actual local corrosion potential of a biomass fired boiler (38 MW_{th} , $453\text{ }^{\circ}\text{C}$ live steam temperature) under full load conditions. To consider the effects of an inhomogeneous flow field in the heat exchangers on the heat transfer and therefore, the local steel temperatures, a finite cell based heat exchanger model was applied in the CFD simulations. Furthermore, two additional cases have been simulated to determine the influences of enhanced steam temperatures and a switch of the steam flow through the final superheater on the high temperature corrosion potential.

The simulations show a rather low corrosion potential for the final superheater under the actual full load conditions. This is in agreement with long-term observations of the plant operator. Furthermore, the simulations show that an increase of the final steam temperature from $453\text{ }^{\circ}\text{C}$ to $480\text{ }^{\circ}\text{C}$ increases the maximum corrosion potential calculated by a factor of 7.4. A change of the flow direction of the final superheater leads to a 3.4 times higher corrosion potential.

Generally, an evenly distributed flow profile over the cross section of the superheater inlet can reduce the local corrosion potential considerably.

Concluding, the empirical model developed allows a comparison of the local corrosion potential of different live steam temperatures, plant geometries or interconnections of the superheater tube bundles. Furthermore, the empirical model allows for a quick estimation if high temperature corrosion is of relevance for a certain plant or not when using a low alloy steel like 13CrMo4-5 and comparable flue gas compositions.

The model is able to roughly estimate the local corrosion potential together with a CFD simulation of flow and heat transfer in a relatively short time and without detailed knowledge of the underlying chemical processes already in the design phase of a plant and hence is a helpful tool for boiler manufacturers.

Acknowledgments

The financial support by the Austrian Ministry for Transport, Innovation and Technology (BMVIT) (program: ModSim: project number: 828703) as well as by the companies BIOS BIOENERGIESYSTEME GmbH, KWB Kraft und Wärme aus Biomasse GmbH, POLYTECHNIK Luft-und Feuerungstechnik GmbH and Josef Bertsch GmbH & Co. is gratefully acknowledged. The online corrosion probe measurements were performed in cooperation with CORR MORAN GmbH, Germany.

REFERENCES

- [1] Li YS, Spiegel M, Shimada S. Corrosion behaviour of various model alloys with NaCl-KCl coating. *Mater Chem Phys* 2005;93(1):217–23.

Table 10 – Maximum values of the calculated corrosion potential for superheater 3.

	Unit	CS1	CS2	CS3
Max(corr.pot.)	$\text{mm}\cdot\text{h}^{-1}$	$7\cdot 10^{-6}$	$2.5\cdot 10^{-5}$	$5.5\cdot 10^{-5}$

- [2] Lehmusto J, Lindberg D, Yrjas P, Skrifvars BJ, Hupa M. The role of potassium in high temperature corrosion of superheater steels. In: Electric Power Research Institute 532 (EPRI), editor. Proceedings of the international conference Impacts of Fuel Quality on Power Production and Environment; 23–27 Sept 2012; Puchberg, Austria. Palo Alto, CA: Electric Power Research Institute 532 (EPRI); 2013.
- [3] Uusitalo MA, Vuoristo PMJ, Mäntylä TA. High temperature corrosion of coatings and boiler steels below chlorine-containing salt deposits. *Corros Sci* 2004;46(6):1311–31.
- [4] Grabke HJ, Reese E, Spiegel M. The effects of chlorides, hydrogen chloride, and sulfur dioxide in the oxidation of steels below deposits. *Corros Sci* 1995;37(7):1023–43.
- [5] Jonsson T, Folkesson N, Svensson JE, Johansson LG, Halvarsson M. An ESEM in situ investigation of initial stages of the KCl induced high temperature corrosion of a Fe2.25Cr1Mo steel at 400 °C. *Corros Sci* 2011;53(6):2233–46.
- [6] Frandsen FJ. Utilizing biomass and waste for power production - a decade of contributing to the understanding, interpretation and analyses of deposits and corrosion products. *Fuel* 2005;84(10):1277–94.
- [7] Obernberger I, Brunner T. Depositionen und Korrosion in Biomassefeuerungen. In: VDI Wissensforum GmbH, editor. Tagungsband zur VDI-Fachkonferenz: Beläge und Korrosion in Großfeuerungsanlagen; June 2004; Göttingen, Germany. Düsseldorf, Germany: VDI-Wissensforum GmbH; 2004.
- [8] Montgomery M, Jensen SA, Borg U, Biede O, Vilhelmsen T. Experiences with high temperature corrosion at straw-firing power plants in Denmark. *Mater Corros* 2011;62(7):593–605.
- [9] Hansen L, Nielsen H, Frandsen F, Dam-Johansen K, Karlsson A. Influence of deposit formation on corrosion at a straw-fired boiler. *Fuel Process Tech* 2000;64(1):189–209.
- [10] Gruber T, Schulze K, Scharler R, Obernberger I. Investigation of the corrosion behaviour of 13CrMo4-5 for biomass fired boilers with coupled online corrosion and deposit probe measurements. *Fuel* 2015 Mar;144:15–24.
- [11] Waldmann B. Korrosion in Anlagen zur thermischen Abfallverwertung: Elektrochemische Korrosionserfassung und Modellbildung [PhD thesis]. Augsburg, Germany: University of Augsburg; 2007.
- [12] Retschitzegger S, Brunner T, Obernberger I, Waldmann B. Assessment of online corrosion measurements in combination with fuel analyses and aerosol and deposit measurements in a biomass combined heat and power plant. *Energy Fuel* 2013;27(10):5670–83.
- [13] Maisch S. Identifikation und Quantifizierung von Korrosionsrelevanten Parametern in Müllverbrennungsanlagen mittels Charakterisierung der deponierten Partikel und elektrochemischer Online-Messungen [PhD thesis]. Augsburg, Germany: University of Augsburg; 2011.
- [14] Gellings PJ, Tostmann KH. Korrosion und Korrosionsschutz von Metallen: eine Einführung. München, Germany: Carl Hanser Verlag; 1981. ISBN: 3-446-12594-9.
- [15] Scharler R, Forstner M, Braun M, Brunner T, Obernberger I. Advanced CFD analysis of large fixed bed biomass boilers with special focus on the convective section. In: ETA-Florence & WIP Munich, editor. Proceedings of the 2nd World Conference and Exhibition on Biomass for Energy, Industry and Climate Protection; 10–14 May 2004; Rome, Italy. Florence, Italy: ETA-Florence; 2004. p. 1357–60. ISBN: 88-89407-04-2.
- [16] Idelchik I. Handbook of hydraulic resistance. 3rd ed. New York, USA: Begell House; 1996. ISBN: 1-56700-074-6.
- [17] VDI. VDI-wärmeatlas. 10. Auflage. Berlin, Germany: Springer-Verlag; 2006. ISBN: 978-3-540-25504-8.
- [18] Zukauskas A, Ulinskas R. High-performance single-phase heat exchangers. Washington DC, USA: Hemisphere Publishing Corporation; 1989. ISBN: 0891167153.